Contribution from the Departments of Chemistry and Radiology, Emory University, Atlanta, Georgia 30322, and Department of Chemistry, University of Siena, I-53100 Siena, Italy

Rhenium(V) Oxo Complexes Relevant to Technetium Renal Imaging Agents Derived from Mercaptoacetylglycylglycylaminobenzoic Acid Isomers. Structural and Molecular Mechanics Studies

Lory Hansen,[†] Renzo Cini,[‡] Andrew Taylor, Jr.,*[,†] and Luigi G. Marzilli*[,†]

Received September 26, 1991

The synthesis and characterization of three rhenium(V) oxo complexes derived from isomers of mercaptoacetylglycylglycylaminobenzoic acid (MAG_2-$ABAH_5$) are reported. The isomers were synthesized from *o*-, *m*- and *p*-aminobenzoic acid and differed in the position of the terminal carboxyl group. The anions of **8**-**10**, $[ReO(MAG_2$-*$ABAH)]^-$ (* = para (**8**), meta (**9**), ortho (**10**)), contained the tetraanionic form of the ligands with the carboxyl group protonated. **8**, **9**, and **10** were synthesized by exchange reactions of $ReOCl_3(Me_2SO)(Ph_3P)$ under moderate conditions and were isolated as $[Ph_4P]^+$, $[Bu_4N]^+$, and $[Ph_4P]^+$ salts, respectively. The structures of **8** and **10** were determined by X-ray diffraction methods; except for the location of the carboxyl group, the structures are similar. The coordination geometry is pseudo square pyramidal, with nitrogen and sulfur donor atoms forming a square base and the oxo ligand at the apex. The orientation of the carboxyl group in **10** is anti to the Re=O group. Crystal data for **8**: chemical formula $C_{37}H_{33}N_3O_7PReS$, a = 10.985 (5) Å, b = 12.320 (5) Å, c = 14.417 (8) Å, α = 93.67 (4)°, β = 106.63 (4)°, γ = 104.78 (3)°, V = 1787.9 (14) Å^3, triclinic, space group $P\bar{1}$, Z = 2. Crystal data for **10**: chemical formula $C_{37}H_{31}N_3O_6PReS$, a = 11.066 (4) Å, b = 19.436 (7) Å, c = 16.495 (6) Å, β = 107.73 (3)°, V = 3379.4 (11) Å^3, monoclinic, space group $P2_1/c$, Z = 4. Since the carboxyl groups are protonated in **8** and **10** and in other relevant structures from this class of radiopharmaceuticals including $[Ph_4As][TcO(MAG_3H)]$ (MAG_3H = tetraanionic form of mercaptoacetyltriglycine), we developed molecular mechanics parameters that allowed us to calculate the structures of **8**, **10**, and $[TcO(MAG_3H)]^-$. We then extended the calculations to all three isomeric complexes in their deprotonated forms and to $[TcO(MAG_3)]^{2-}$ in order to approximate their solution phase structures. We conclude that the $[TcO(MAG_3)]^{2-}$ species is conformationally flexible, and we have made an initial assessment of structures vs renal clearance.

Introduction

The N_3S (triamide monothiol) ligand system forms complexes with both Tc and Re radionuclides; these complexes have applications in nuclear medicine. $[^{99m}TcO(MAG_3)]^{2-}$ (MAG_3 = pentaanionic form of mercaptoacetyltriglycine in which the mercapto, amide, and carboxyl groups are deprotonated) is widely used clinically as a renal radiopharmaceutical.[1] $[^{99m}TcO(MAG_3)]^{2-}$ and $[^{186}Re/^{188}ReO(MAG_3)]^{2-}$ derivatives have been conjugated with antibodies and are now are being investigated for the detection and therapy of cancer.[2,3]

A rapid renal clearance is a desirable property for a new ^{99m}Tc renal agent, but it is also important that the labeled metabolites of ^{99m}Tc and $^{186}Re/^{188}Re$ labeled proteins and antibodies be cleared rapidly from the body. Subtle changes in the structures of these metal complexes have a profound effect on their route and rate of excretion, and further understanding of structure–distribution relationships requires crystal structure determinations of related complexes.[4] The crystal structures of $[Ph_4As][^{99}TcO(MAG_3H)]$[5] ($^{99}Tc$, $t_{1/2}$ = 2.12 × 10^5 years) and $[Bu_4N][ReO(MAG_3H)]$[2] (where MAG_3H is a tetraanionic form and differs from MAG_3 in having a protonated carboxyl group) have been determined; however, fully refined structural details have not been presented. Structures of other Tc–N_3S or Re–N_3S complexes have not been reported. This dearth of structural information is striking in consideration of the large number of $MO(MAG_3)$ (M = Tc, Re) derivatives that have been synthesized and evaluated biologically.[6-8]

$[^{99m}TcO(MAG_3)]^{2-}$ is a dianionic complex with one charge associated with the metal core and the second associated with the terminal carboxyl group that is ionized at physiological pH. Previous studies of $[^{99m}TcO(MAG_3)]^{2-}$ analogues indicate that the presence and position of the uncoordinated, deprotonated carboxyl group is important for efficient renal clearance.[6,9,10] For example, $[TcO(mae)]^-$ (mae = tetraanionic 1,2-bis(mercaptoacetamido)ethylene) which lacks a carboxyl group is excreted at only half the rate of *syn*-$[^{99m}TcO(map)]^{2-}$ (map = pentaanionic 2,3-bis(mercaptoacetamido)propanoate) in humans.[10] However, $[TcO(mae)]^-$ is excreted somewhat more rapidly than *anti*-$[^{99m}TcO(map)]^{2-}$. Syn and anti refer to the orientation of the carboxyl group with respect to the oxo ligand. Unfortunately, the orientation of the carboxyl group is different in the solid-state structures of $[TcO(MAG_3H)]^-$[5] and $[ReO(MAG_3H)]^-$.[2] The orientation is syn in the Tc complex and anti in the Re complex. In addition, crystal structural data show that $[TcO(MAG_3H)]^-$,[5] $[ReO(MAG_3H)]^-$,[2] $[TcO(mapH)]^-$, and $[ReO(mapH)]^-$[4] all have protonated carboxyl groups.

Our work has focused on the development of a second-generation ^{99m}Tc renal radiopharmaceutical based on the prototype agent $[^{99m}TcO(MAG_3)]^{2-}$. In order to design a $[^{99m}TcO(MAG_3)]^{2-}$ derivative with a more rapid renal clearance, it is essential to understand how the position of the carboxyl group influences renal excretion. Kidneys efficiently extract a variety of organic anions from plasma via cellular transport. Free anions bind to transport receptors located within the peritubular plasma membrane of renal tubular cells. The receptors transport the anions across the cell membrane into the cytoplasm. This process elevates the intracellular anionic concentration, which promotes diffusion of the anions into the urine through a preferentially permeable luminal membrane. The efficiency of the transport mechanism depends on the interaction of the anionic species with the transport receptor. The structural requirements favoring this interaction have not been completely elucidated, but a carbonylglycine unit ($-CO-NH-CH_2-COO^-$) has been implicated as important for efficient tubular secretion.[11]

[†] Emory University.
[‡] University of Siena.

(1) Eshima, D.; Fritzberg, A. R.; Taylor, A., Jr. *Semin. Nucl. Med.* **1990**, *20*, 28.
(2) Rao, T. N.; Adhikesavalu, D.; Camerman, A.; Fritzberg, A. R. *Inorg. Chim. Acta* **1991**, *180*, 63.
(3) Axworthy, D. B.; Sue, F.-M.; Vanderheyden, J.-L.; Srinivasan, A.; Fitzner, J.; Galster, G.; Beaumier, P.; Fritzberg, A. R. *J. Nucl. Med.* **1991**, *32*, 915 (abstract).
(4) Rao, T. N.; Adhikesavalu, D.; Camerman, A.; Fritzberg, A. R. *J. Am. Chem. Soc.* **1990**, *112*, 5798.
(5) (a) Nosco, D. L.; Manning, R. G. *J. Nucl. Med.* **1986**, *27*, 939 (abstract). (b) Nosco, Dennis, Ph. D. Mallinkrodt, Inc. Unpublished data (cited with permission).
(6) Kasina, S.; Fritzberg, A. R.; Johnson, D. L.; Eshima, D. *J. Med. Chem.* **1986**, *29*, 1933.
(7) Eshima, D.; Taylor, A., Jr.; Fritzberg, A. R.; Kasina, S.; Hansen, L.; Sorenson, J. F. *J. Nucl. Med.* **1987**, *28*, 1180.
(8) Borman, Guy. *Synthesis, Labeling Characteristics and Biological Evaluation of Technetium-99m Complexes for Renal Function Imaging*; Katholieke Universiteit Leuven: Leuven, Belgium, 1990 (dissertation).
(9) Fritzberg, A. R.; Kuni, C. C.; Klingensmith, W. C., III; Stevens, J.; Whitney, W. P. *J. Nucl. Med.* **1982**, *23*, 592.
(10) Fritzberg, A. R. *J. Nucl. Med. Tech.* **1984**, *4*, 177.
(11) Despopoulos, A. *J. Theor. Biol.* **1965**, *8*, 163.

0020-1669/92/1331-2801$03.00/0

In this study, we designed analogues to vary the position of the carboxyl group and simultaneously restrict its mobility by introducing a rigid aromatic group between it and the metal coordination sphere. In these analogues, we replaced the terminal glycine of the mercaptoacetyltriglycine ligand with *o*-, *m*-, and *p*-aminobenzoic acid, which upon coordination give complexes of the fully deprotonated pentaanionic forms of mercaptoacetylglycylglycylaminobenzoic acids, MAG_2-oABA, MAG_2-mABA, and MAG_2-pABA, respectively.

The renal clearance of ^{99m}Tc complexes with these ligands has been measured in rats.[12] The renal clearance of the para isomer is rougly three times greater than the meta and ortho isomers. Clearly, the para isomer is unique within this series with respect to its ability to interact with the renal anion transport mechanism.

Re complexes were prepared with the MAG_2-ABA ligands as structural models for the Tc complexes because Tc and Re complexes with identical ligands have essentially identical coordination parameters[13] and Re is an environmentally preferable, nonradioactive element. The solid-state structures of $[Ph_4P][ReO(MAG_2\text{-}oABAH)]$ and $[Ph_4P][ReO(MAG_2\text{-}pABAH)]$ were determined by X-ray diffraction. Again, the carboxyl groups are protonated in these crystalline derivatives. Therefore, we developed a force field that allowed us to calculate the geometry of the protonated species by molecular mechanics methods. With this information, we could predict the structures of all three isomers in their deprotonated, more physiologically relevant forms. We also developed parameters for Tc(V) oxo complexes and calculated the structures of the deprotonated forms of $[TcO(MAG_3)]^{2-}$.

Experimental Section

NMR spectra were obtained at 300 MHz for ^1H and 75 MHz for ^{13}C with a General Electric QE-300 spectrometer. All spectra were recorded in Me_2SO-d_6. Chemical shifts (ppm) were referenced to the solvent peak 2.49 ppm (^1H) and 39.9 ppm (^{13}C) vs TMS (tetramethylsilane). Elemental analyses were performed by Atlantic Microlabs Inc., Atlanta, GA. Visible spectra were recorded with a Perkin-Elmer Lambda 3A spectrophotometer and the FTIR spectra were recorded with a Bruker IFS 66 instrument. Yields are based on purified, air-dried material. Analytical and ^1H NMR data for **1**–**6** are available as supplementary material.

Ligand Synthesis. Phthaloylglycyl chloride[14] (PGC) and succinimidyl-*N*-((benzoylthio)acetyl)glycinate[15] (SBzMAG-OSucc) were prepared by literature methods.

Glycyl-*p*-aminobenzoic Acid Hydrochloride (1). The preparation of **1** was based on a reported method.[14] *p*-Aminobenzoic acid (7.95 g, 0.058 mol) and MgO (1.2 g, 0.030 mol) were suspended in H_2O (150 mL) and cooled to 5 °C. PGC (6.42 g, 0.029 mol) in dioxane (50 mL) was added dropwise to the aqueous suspension over 45 min. After the reaction mixture had been stirred for 1 h it was brought to pH 1 with concentrated HCl. The solid was collected and washed with boiling EtOH. The resulting phthaloylglyclyl-*p*-amidobenzoic acid (6.10 g, 0.020 mol) was deprotected by refluxing in alcoholic hydrazine hydrate (250 mL, 0.1 M) for 2 h. After the solvent was rotary evaporated, the product was dissolved in 2 N HCl (200 mL) by warming to 60 °C for 30 min. Phthalohydrazide was removed by filtration and the filtrate was refrigerated overnight. The resulting precipitate was collected and recrystallized from H_2O. Yield: 1.83 g (27%).

Glycyl-*m*-aminobenzoic Acid Hydrochloride (2) and Glycyl-*o*-aminobenzoic Acid Hydrochloride (3). These were prepared as described above for **1** with *m*-aminobenzoic acid (9.60 g, 0.070 mol) and anthranilic acid (9.60 g, 0.070 mol), respectively, along with MgO (1.61 g, 0.040 mol) and PGC (7.83 g, 0.035 mol). They were recrystallized from MeOH. Yields: **2**, 1.85 g (23%); **3**, 1.80 g (22%).

***N*-((Benzoylthio)acetyl)glycylglycyl-*p*-aminobenzoic Acid (4).** **1** (0.92 g, 4.0 mmol) was dissolved in 80% MeOH/H_2O (50 mL) with warming and adjusting the pH to 8 with dropwise addition of 1 N NaOH. SBzMAG-OSucc (1.55 g, 4.4 mmol) was added and the solution was heated at reflux for 2 h and stirred at room temperature for 4 h. The volume was reduced in half by rotary evaporation. The crude product was collected and recrystallized from iPrOH/H_2O. Yield: 1.30 g (76%). ^{13}C NMR: 190.54 (CO), 169.34 (CO), 168.33 (CO), 167.77 (CO), 167.07 (CO), 142.97 (ArC), 136.11 (SBzC), 134.30 (SBzC), 130.59 (2 C, ArC), 129.35 (2 C, SBzC), 127.10 (2 C, SBzC), 125.43 (ArC), 118.61 (2 C, ArC), 43.02 (NCH_2), 42.84 (NCH_2), 32.65 (SCH_2).

***N*-((Benzoylthio)acetyl)glycylglycyl-*m*-aminobenzoic Acid (5).** This compound was prepared as described above for **4** with **2** (1.43 g, 6.2 mmol) and SBzMAG-OSucc (2.72 g, 7.8 mmol). Yield: 1.25 g (47%). ^{13}C NMR: 190.55 (CO), 169.30 (CO), 168.04 (CO), 167.70 (CO), 167.28 (CO), 139.14 (ArC), 136.10 (SBzC), 134.28 (SBzC), 131.47 (ArC), 129.34 (2 C, SBzC), 129.18 (ArC), 127.09 (2 C, SBzC), 124.34 (ArC), 123.50 (ArC), 120.15 (ArC), 42.91 (NCH_2), 42.81 (NCH_2), 32.67 (SCH_2).

***N*-((Benzoylthio)acetyl)glycylglycyl-*o*-aminobenzoic Acid (6).** This compound was prepared as described above for **4** with **3** (0.53 g, 2.3 mmol) and SBzMAG-OSucc (0.89 g, 2.5 mmol). It was crystallized from iPrOH. Yield: 0.64 g (65%). ^{13}C NMR: 190.50 (CO), 169.79 (CO), 169.75 (CO), 168.57 (CO), 167.34 (CO), 140.68 (ArC), 136.11 (SBzC), 134.55 (ArC), 134.29 (SBzC), 131.47 (ArC), 129.37 (2 C, SBzC), 127.08 (2 C, SBzC), 123.05 (ArC), 119.50 (ArC), 116.17 (ArC), 43.90 (NCH_2), 42.66 (NCH_2), 32.59 (SCH_2).

Synthesis of Rhenium(V) Complexes. $ReOCl_3(Me_2SO)(Ph_3P)$ (7). This complex was prepared by the method of Grove and Wilkinson.[16] FTIR in KBr: 992 cm^{-1} [Re=O], 1139, 1126 cm^{-1} [S—O] (lit. 981 cm^{-1} [Re=O], 1138, 1129 cm^{-1} [S—O]).

$[Ph_4P][ReO(mercaptoacetylglycylglycyl\text{-}p\text{-}aminobenzoato)]\cdot H_2O$ (8). **4** (0.37 g, 0.86 mmol) was dissolved in 62% MeOH/H_2O (16 mL) with warming and adjusting the pH to 8 with 1 N NaOH. **7** (0.40 g, 0.62 mmol) was added to the solution to give a green suspension which was heated to 65–70 °C. As the reaction proceeded, a pH of 8 was maintained by dropwise addition of 1 N NaOH. The green suspension gradually cleared to give an orange solution after 1 h. The solution was cooled to room temperature, filtered, and extracted twice with $CHCl_3$. Tetraphenylphosphonium bromide (0.36 g, 0.86 mmol) was added to the orange solution, and the pH of the solution was adjusted to 5 with 1 N HCl. The product was extracted into $CHCl_3$ and the $CHCl_3$ evaporated in a hood. The oily residue was crystallized from 20% MeOH/H_2O. Yield: 0.22 g (40%). Single crystals were obtained with diluting a saturated solution of the complex in EtOH with H_2O (four times). Long flat crystals formed at room temperature over 2–3 days. Anal. Calcd for $C_{37}H_{33}N_3O_7PReS$: C, 50.45; H, 3.78; N, 4.77. Found: C, 50.53; H, 3.74; N, 4.80. ^1H NMR: 7.95 (m, 4 H, phenyl), 7.87 (d, 2 H, J = 8 Hz, ArH), 7.77 (m, 16 H, phenyl), 7.17 (d, 2 H, J = 8 Hz, ArH), 4.58, 4.16 (dd, 2 H, J = 18 Hz, NCH_2), 4.39, 4.21 (dd, 2 H, J = 18 Hz, NCH_2), 3.61, 3.52 (dd, 2 H, J = 17 Hz, SCH_2). ^{13}C NMR: 192.17 (CONH), 189.23 (CONH), 188.24 (CONH), 167.28 (COOH), 157.01 (ArC), 135.52 (d, J = 2 Hz, phenyl), 134.75 (d, J = 10 Hz, phenyl), 130.63 (d, J = 13 Hz, phenyl), 129.19 (2 C, ArC), 127.95 (2 C, ArC), 127.00 (ArC), 117.87 (d, J = 90 Hz, phenyl), 55.87 (NCH_2), 53.70 (NCH_2), 38.18 (SCH_2). Visible spectrum in CH_3CN: λ_{max}, nm (ϵ, M^{-1} cm^{-1}) 400 (211) 483 (29). FTIR in KBr: 970 cm^{-1} [Re=O].

$[Bu_4N][ReO(mercaptoacetylglycylglycyl\text{-}m\text{-}aminobenzoato)]\cdot H_2O$ (9). This complex was prepared as described for **8** with **5** (0.27 g, 0.63 mmol) and **7** (0.30 g, 0.46 mmol) except that tetrabutylammonium bromide was used to provide the counterion. The product was crystallized from 10% EtOH/H_2O. Yield: 0.13 g (37%). Anal. Calcd for $C_{29}H_{49}N_4O_7ReS$: C, 44.43; H, 6.30; N, 7.15. Found: C, 44.47; H, 6.32; N, 7.14. ^1H NMR: 7.67 (d, 1 H, J = 8 Hz, ArH), 7.66 (s, 1 H, ArH), 7.30 (d, 1 H, J = 8 Hz, ArH), 4.59, 4.17 (dd, 2 H, J = 18 Hz, NCH_2), 4.39, 4.21 (dd, 2 H, J = 18 Hz, NCH_2), 3.63, 3.53 (dd, 2 H, J = 17 Hz, SCH_2), 3.14 (m, 8 H, $N(CH_2)_4$ butyl), 1.55 (m, 8 H, $(CH_2)_4$ butyl), 1.29 (m, 8 H, $(CH_2)_4$ butyl), 0.91 (m, 12 H, $(CH_3)_4$ butyl). ^{13}C NMR: 192.20 (CONH), 189.45 (CONH), 188.26 (CONH), 167.51 (COOH), 152.86 (ArC), 132.29 (ArC), 130.55 (ArC), 128.77 (ArC), 127.98 (ArC), 125.76 (ArC), 57.70 ($N(CH_2)_4$ butyl), 55.89 (NCH_2), 53.59 (NCH_2), 38.21 (SCH_2), 23.23 ($(CH_2)_4$ butyl), 19.39 ($(CH_2)_4$ butyl), 13.66 ($(CH_3)_4$ butyl). Visible spectrum in CH_3CN: λ_{max}, nm (ϵ, M^{-1} cm^{-1}) 400 (176), 483 (25). FTIR in KBr: 977 cm^{-1} [Re=O].

$[Ph_4P][ReO(mercaptoacetylglycylglycyl\text{-}o\text{-}aminobenzoato)]$ (10). This complex was prepared as described above for **8** with **6** (0.37 g, 0.86 mmol) and **7** (0.40 g, 0.63 mmol). The product was crystallized from 40% MeOH/H_2O. Yield: 0.21 g (38%). Recrystallization from EtOH produced long flat hexagonal crystals. Anal. Calcd for $C_{37}H_{31}N_3O_6PReS$: C, 51.50; H, 3.62; N, 4.87. Found: C, 51.61; H, 3.65; N, 4.91. ^1H NMR: 7.97 (m, 5 H, ArH and phenyl), 7.81 (m, 16 H, phenyl), 7.53 (t, 1 H, J = 8 Hz, ArH), 7.19 (m, 2 H, ArH), 4.53, 4.16 (dd, 2 H, J = 18 Hz, NCH_2), 4.26, 4.13 (dd, 2 H, J = 18 Hz, NCH_2),

(12) Hansen, L.; Boelrijk, A.; Banaszczyk, M.; Eshima, D.; Malveaux, G.; Marzilli, L. G.; Taylor, A., Jr. Manuscript in preparation.
(13) Deutsch, E.; Libson, K.; Vanderheyden, J.-L. In *Technetium and Rhenium in Chemistry and Nuclear Medicine 3*; Nicolini, M., Bandoli, G., Mazzi, U., Eds.; Cortina International: Verona, Italy, 1990; p 13.
(14) Sheehan, J. C.; Frank, V. S. *J. Am. Chem. Soc.* **1949**, *71*, 1856.
(15) Schneider, R. F.; Subramanian, G.; Feld, T. A.; McAfee, J. G.; Zapf-Longo, C.; Palladino, E.; Thomas, F. D. *J. Nucl. Med.* **1984**, *25*, 223.
(16) Wilkinson, G.; Grove, D. E. *J. Chem. Soc. A* **1966**, 1224.

Table I. Crystallographic Data

	8	10
chem formula	$C_{37}H_{33}N_3O_7PReS$	$C_{37}H_{31}N_3O_6PReS$
fw	880.92	862.91
space group	$P\bar{1}$ (No. 2)	$P2_1/c$ (No. 14)
Z	2	4
a, Å	10.985 (5)	11.066 (4)
b, Å	12.320 (5)	19.436 (7)
c, Å	14.417 (8)	16.495 (6)
α, deg	93.67 (4)	
β, deg	106.63 (4)	107.73 (3)
γ, deg	104.78 (3)	
V, Å^3	1787.9 (14)	3379.4 (11)
d_{calcd}, g/cm^3	1.636	1.696
λ, Å	0.71073	0.71073
μ, mm^{-1}	3.71	3.80
T, °C	25	25
transm coeff	0.024–0.057	0.016–0.035
R	0.038	0.033
R_w	0.042	0.041

3.61, 3.49 (dd, 2 H, J = 17 Hz, SCH_2). ^{13}C NMR: 192.20 (CONH), 190.23 (CONH), 188.26 (CONH), 166.95 (COOH), 153.88 (ArC), 135.52 (phenyl), 134.75 (d, J = 11 Hz, phenyl), 132.71 (ArC), 130.64 (d, J = 12 Hz, phenyl), 130.07 (ArC), 129.98 (ArC), 127.71 (ArC), 125.00 (ArC), 117.37 (d, J = 88 Hz, phenyl), 55.96 (NCH_2), 53.79 (NCH_2), 38.43 (SCH_2). FTIR in KBr: 966 cm^{-1} [Re=O].

X-ray Crystallography. Orange crystals of **8** and **10** having approximate dimensions of 0.59 × 0.32 × 0.20 mm and 0.80 × 0.32 × 0.16 mm, respectively, were mounted on glass fibers. **8** was sealed in cyanoacrylate ester to prevent desolvation. Data collection was performed on a Nicolet P3F diffractometer. Approximate cell parameters and orientation matrices were calculated from least-squares refinement of 25 reflections identified from rotation photographs. Two additional sets of high angle (2θ) reflections were used for obtaining refined cell constants: 23–36°, 31–36° for **8** and 35–37°, 33–40° for **10**. Two to three check reflections were measured every 2 h, and there was no significant decrease in the intensities. Intensities were corrected for Lorentz–polarization effects (including monochromator polarization) and absorption based on azimuthal scans of five to six reflections. The structures were solved by Patterson methods, and all non-hydrogen atoms were refined anisotropically by full-matrix least-squares procedures. The carboxyl and water hydrogen atoms were located from difference maps and included in the calculations. The methylene and aromatic hydrogen atoms were included at calculated (d(C–H) = 0.96 Å) positions. All hydrogen atoms were assigned isotropic thermal parameters as follows; (**8**) the carboxyl and water hydrogen atoms were fixed at 10% and the methylene and aromatic hydrogen atoms were assigned isotropic thermal parameters that were 20% greater than the U_{equiv} of carbon to which they were bonded; (**10**) all hydrogen atoms were fixed at 8%. The values for the thermal parameters of the hydrogen atoms were chosen differently because different programs were used (see below). The maximum peaks in the final difference maps were 1.6 and 1.1 e/Å^3 (located 0.98 and 1.62 Å from Re) for **8** and **10**, respectively.

SHELXTL, SHELXS-86, and SHELX-76 computer programs were used for the structure solution and refinement of **8** with scattering factors taken from ref 17 (Re atom), Cromer and Mann[18] (all other non-hydrogen atoms), and Stewart, Davidson, and Simpson[19] (H atoms). Anomalous dispersion corrections were taken from ref 17 (Re atom) and Cromer and Liberman[20] (all other non-hydrogen atoms). The SHELXTL PLUS computer program was used for the structure solution and refinement of **10**. Scattering factors and anomalous dispersion corrections were taken from ref 17. Crystallographic data are presented in Table I and final atomic coordinates are presented in Tables II and III for **8** and **10**, respectively. The supplementary material includes a full tabular presentation of the crystallographic studies.

Molecular Mechanics Investigation on Rhenium(V) and Technetium(V) Complexes. The strain energies of the complexes were computed as the sum of the bond length deformation (E_b), valence angle deformation (E_θ), torsional angle deformation (E_ϕ), nonbonding interaction (E_{nb}) and hydrogen bond interaction (E_{hb}) contributions:

$$E_{tot} = E_b + E_\theta + E_\phi + E_{nb} + E_{hb}$$

Table II. Atomic Coordinates (×10^4) and Equivalent Isotropic Displacement Coefficients for $[Ph_4P][ReO(MAG_2\text{-}pABAH)]\cdot H_2O$ (**8**)

atom	x	y	z	U_{equiv},[a] Å^2
Re	1029 (1)	3469 (1)	3672 (1)	46 (1)
S	1741 (2)	5152 (2)	4696 (1)	53 (1)
N(1)	336 (5)	4405 (5)	2693 (4)	50 (2)
N(2)	1418 (6)	2885 (5)	2507 (4)	55 (2)
N(3)	2738 (5)	3082 (5)	4289 (4)	56 (2)
O(1)	−221 (5)	2573 (4)	3919 (4)	63 (2)
O(2)	−248 (6)	6011 (5)	2272 (4)	75 (3)
O(3)	807 (6)	2638 (5)	832 (4)	71 (2)
O(4)	4160 (6)	2112 (5)	3988 (5)	82 (3)
O(5)	5078 (6)	4043 (5)	8985 (4)	79 (3)
O(6)	6823 (6)	4888 (7)	8560 (4)	98 (3)
C(1)	718 (8)	5945 (6)	3957 (5)	59 (3)
C(2)	224 (7)	5459 (6)	2897 (5)	55 (3)
C(3)	29 (8)	3938 (7)	1664 (5)	60 (3)
C(4)	786 (7)	3096 (6)	1617 (5)	57 (3)
C(5)	2437 (8)	2300 (7)	2633 (6)	69 (3)
C(6)	3202 (7)	2461 (6)	3698 (6)	58 (3)
C(7)	3476 (7)	3367 (5)	5316 (5)	49 (2)
C(8)	4855 (7)	3891 (6)	5623 (5)	59 (3)
C(9)	5524 (7)	4208 (7)	6614 (5)	61 (3)
C(10)	4866 (7)	4003 (6)	7298 (5)	58 (3)
C(11)	3495 (7)	3484 (5)	6990 (5)	52 (3)
C(12)	2832 (7)	3182 (6)	5999 (5)	52 (3)
C(13)	5577 (8)	4315 (7)	8372 (6)	65 (3)
P	−3723 (2)	342 (2)	2487 (1)	48 (1)
C(14)	−5432 (7)	−489 (6)	2092 (5)	52 (3)
C(15)	−5786 (7)	−1484 (6)	2468 (6)	61 (3)
C(16)	−7079 (8)	−2179 (7)	2139 (7)	74 (4)
C(17)	−8017 (9)	−1880 (9)	1440 (8)	93 (5)
C(18)	−7666 (9)	−885 (10)	1060 (8)	98 (5)
C(19)	−6392 (8)	−216 (8)	1383 (7)	81 (4)
C(20)	−3573 (6)	1742 (6)	2168 (5)	52 (3)
C(21)	−3768 (8)	1876 (7)	1197 (6)	68 (3)
C(22)	−3743 (8)	2938 (7)	911 (7)	74 (4)
C(23)	−3469 (9)	3855 (7)	1599 (7)	75 (4)
C(24)	−3252 (10)	3720 (7)	2570 (7)	81 (4)
C(25)	−3294 (8)	2686 (7)	2855 (6)	68 (3)
C(26)	−2825 (7)	−295 (6)	1842 (5)	53 (3)
C(27)	−3386 (8)	−1364 (6)	1317 (6)	62 (3)
C(28)	−2682 (9)	−1805 (7)	802 (7)	75 (4)
C(29)	−1441 (9)	−1164 (8)	822 (7)	77 (4)
C(30)	−897 (8)	−103 (8)	1358 (7)	79 (4)
C(31)	−1569 (8)	343 (6)	1873 (6)	69 (3)
C(32)	−3069 (6)	349 (6)	3783 (5)	51 (3)
C(33)	−3663 (8)	798 (7)	4387 (6)	67 (3)
C(34)	−3194 (10)	808 (9)	5377 (7)	86 (5)
C(35)	−2166 (11)	361 (9)	5754 (7)	89 (5)
C(36)	−1604 (9)	−107 (9)	5174 (7)	84 (4)
C(37)	−2054 (7)	−116 (7)	4159 (6)	63 (3)
O(7)	−1578 (7)	5751 (6)	314 (4)	96 (3)

[a] Equivalent isotropic U defined as one-third of the trace of the orthogonalized U_{ij} tensor.

As usual for metal–ligand complexes, the electrostatic interaction contribution was not included in the calculation.[21-26] The force field used for the ligand part of the complexes was Amber,[27] contained in the MacroModel package, Version 3.0 ("final value quality").[28] Substantial

(17) *International Tables for X-ray Crystallography*; Kynoch Press: Birmingham, 1974; Vol IV.
(18) Cromer, D. T.; Mann, J. B. *Acta Crystallogr.* **1968**, *A24*, 321.
(19) Stewart, R. F.; Davidson, E. R.; Simpson, W. T. *J. Chem. Phys.* **1965**, *42*, 3175.
(20) Cromer, D. T.; Liberman, D. *J. Chem. Phys.* **1970**, *53*, 1891.
(21) McDougall, G. J.; Hancock, R. D.; Boeyens, J. C. A. *J. Chem. Soc., Dalton Trans.* **1978**, 1438.
(22) Buckingham, D. A.; Creswell, P. J.; Dellaca, R. J.; Dwyer, M.; Gainsford, G. L.; Marzilli, L. G.; Maxwell, I. E.; Robinson, W. T.; Sargeson, A. M.; Turnbull, K. R. *J. Am. Chem. Soc.* **1974**, *96*, 1713.
(23) Boyens, J. C.; Cotton, F. A.; Han, S. A. *Inorg. Chem.* **1985**, *24*, 1750.
(24) Harding, C.; McDowell, D.; Nelson, J.; Raghunathan, S.; Stevenson, C. *J. Chem. Soc., Dalton Trans.* **1990**, 2521.
(25) Hancock, R. D.; Dobson, S. M.; Evers, A.; Wade, P. W.; Ngwenya, M. P.; Boyens, J. C.; Wainwright, K. P. *J. Am. Chem. Soc.* **1988**, *110*, 2788.
(26) Adam, K. R.; McCool, B. J.; Leong, A. J.; Lindoy, L. F.; Ansel, C. W. G.; Baillie, P. J.; Dacey, K. P.; Drummond, L. A.; Hedrick, K.; McPartlin, M. *J. Chem. Soc., Dalton Trans.* **1990**, 3435.
(27) (a) Weiner, S. J.; Kollman, P. A.; Case, D. A.; Singh, U. C.; Ghio, C.; Alagona, G.; Profeta, S., Jr.; Weiner, P. *J. Am. Chem. Soc.* **1984**, *106*, 765. (b) Weiner, S. J.; Kollman, P. A.; Nguyen, D. T.; Case, D. A. *J. Comput. Chem.* **1986**, *7*, 230.

Table III. Atomic Coordinates ($\times 10^4$) and Equivalent Isotropic Displacement Coefficients for $[Ph_4P][ReO(MAG_2\text{-}oABAH)]$ (**10**)

atom	x	y	z	U_{equiv},[a] Å^2
Re	2171 (1)	4291 (1)	−2628 (1)	39 (1)
S	4081 (2)	3784 (1)	−1941 (1)	52 (1)
N(1)	1539 (5)	3642 (2)	−1897 (3)	42 (2)
N(2)	536 (5)	3991 (3)	−3430 (3)	44 (2)
N(3)	2548 (5)	4305 (2)	−3751 (3)	41 (2)
O(1)	2125 (4)	5106 (2)	−2291 (3)	58 (2)
O(2)	1848 (4)	2950 (2)	−737 (3)	54 (2)
O(3)	−1411 (4)	3508 (3)	−3569 (3)	66 (2)
O(4)	1602 (4)	4393 (2)	−5207 (3)	57 (2)
O(5)	4154 (4)	3227 (3)	−5422 (3)	64 (2)
O(6)	2956 (4)	3052 (2)	−4577 (3)	55 (2)
C(1)	3689 (6)	3398 (4)	−1044 (4)	59 (3)
C(2)	2284 (6)	3306 (3)	−1207 (4)	48 (2)
C(3)	180 (6)	3500 (3)	−2191 (4)	52 (2)
C(4)	−342 (6)	3663 (3)	−3133 (4)	48 (3)
C(5)	287 (6)	4110 (3)	−4333 (4)	48 (2)
C(6)	1541 (6)	4284 (3)	−4489 (4)	43 (2)
C(7)	3786 (6)	4432 (3)	−3827 (4)	41 (2)
C(8)	4424 (6)	5009 (3)	−3416 (4)	48 (2)
C(9)	5627 (6)	5180 (3)	−3455 (4)	54 (3)
C(10)	6210 (6)	4777 (3)	−3908 (4)	57 (3)
C(11)	5588 (6)	4200 (3)	−4320 (4)	51 (3)
C(12)	4374 (6)	4015 (3)	−4296 (4)	43 (2)
C(13)	3812 (6)	3401 (3)	−4820 (4)	47 (2)
P	1779 (2)	−1627 (1)	4467 (1)	41 (1)
C(14)	1798 (6)	−830 (3)	5025 (4)	44 (2)
C(15)	2286 (7)	−823 (3)	5917 (5)	61 (3)
C(16)	2322 (8)	−207 (4)	6360 (5)	78 (3)
C(17)	1927 (7)	393 (4)	5929 (6)	70 (3)
C(18)	1478 (7)	396 (3)	5050 (5)	64 (3)
C(19)	1411 (6)	−216 (3)	4598 (4)	56 (3)
C(20)	3055 (6)	−1625 (3)	4009 (4)	47 (2)
C(21)	3271 (7)	−2203 (4)	3576 (4)	58 (3)
C(22)	4266 (7)	−2210 (4)	3229 (5)	72 (3)
C(23)	5021 (7)	−1626 (5)	3307 (5)	81 (4)
C(24)	4810 (7)	−1054 (5)	3719 (5)	76 (4)
C(25)	3836 (6)	−1049 (4)	4092 (4)	56 (3)
C(26)	289 (5)	−1709 (3)	3618 (4)	41 (2)
C(27)	−659 (6)	−2158 (3)	3672 (4)	47 (2)
C(28)	−1788 (6)	−2191 (3)	3029 (5)	57 (3)
C(29)	−1976 (6)	−1771 (4)	2315 (5)	60 (3)
C(30)	−1034 (7)	−1329 (3)	2252 (4)	58 (3)
C(31)	97 (6)	−1292 (3)	2893 (4)	49 (2)
C(32)	1967 (6)	−2316 (3)	5220 (4)	42 (2)
C(33)	1043 (6)	−2410 (3)	5629 (4)	48 (2)
C(34)	1157 (7)	−2959 (3)	6188 (4)	55 (3)
C(35)	2184 (7)	−3395 (3)	6360 (4)	63 (3)
C(36)	3117 (7)	−3292 (4)	5974 (4)	65 (3)
C(37)	3006 (6)	−2748 (3)	5403 (4)	49 (2)

[a] Equivalent isotropic U defined as one-third of the trace of the orthogonalized U_{ij} tensor.

modification and extension of the force field was necessary to account for the metal center. The proper force field parameters were derived by a trial-and-error procedure, in which the calculated structures reached good agreement with those observed in the solid state by X-ray diffraction analysis of **8** and **10** and the complexes in refs 4 and 29. The starting force field values were those previously reported for some metal complexes.[22,23,25,26] The Re=O and Tc=O stretching force constants were computed from infrared spectral data reported in ref 4 and obtained in the present work. A special substructure file for the force field was created to compute the metal–donor interactions. Good agreement with the X-ray structures was achieved by using the parameters listed in Table IV. The Van der Waals radius adopted for the Re and Tc center is 2.6 Å, which is in agreement with the values of 2.6, 2.5, and 2.35 Å previously used for Rh(II), Cu(II),[23] and Co(II)[24] complexes. The ϵ constant was 1.6 kcal/mol found from a trial-and-error procedure starting from the value of 1.63 kcal/mol reported for Co(II).[24] The calculations were carried out with the computer systems and procedures previously described.[30]

Table IV. Details of the Force Field for Bonds Involving the Metal Center[a]

bond	R_0, Å	K,[b] kcal·Å^2/mol
Re=O	1.66	415
Re—N	1.99	130
Re—O	1.95	130
Re—S	2.29	130
Tc=O	1.66	370
Tc—N	1.99	125
Tc—O	1.95	125
Tc—S	2.29	125

angle	θ_0, deg	K,[c] kcal·rad^2/mol
M—S—C(sp^3)	99.0	30
M—N(sp^2)—C(sp^2)	122.0	30
M—N(sp^2)—C(sp^3)	118.0	30
S—M=O	110.0	49
N(sp^2)—M=O	110.0	49
M—O—C(sp^3)	120.5	30
S—M—S	86.0	49
O—M—O	80.0	49
O—M—S(trans)	140.0	49

Substructure[d]

ZO(=O2)–S1–C3–C2(=O2)–N2(−1)–C3–
1 2 3 4 5 6 7 8

C2(=O2)–N2(−1)–C3–C2(=O2)–N2(−1)–C2
9 10 11 12 13 14 15 16

angle	θ_0, deg	K,[c] kcal·rad^2/mol
3–1–7	84.0	49
3–1–11	136.0	49
3–1–15	92.0	49
7–1–11	78.0	49
11–1–15	78.0	49
7–1–15	139.0	49

torsional terms	V1, kcal/mol	V2, kcal/mol	V3, kcal/mol
M—N(sp^2)—C(sp^2)—C(sp^3)	0.0	0.8	0.0
M—N(sp^2)—C(sp^3)—C(sp^2)	0.0	0.4	0.4
M—N(sp^2)—C(sp^2)—C(sp^2)	0.0	1.5	0.0
M—S—C(sp^3)—C(sp^2)	0.0	0.9	0.1
M—S—C(sp^3)—C(sp^3)	0.0	0.5	0.5
M—O—C(sp^3)—C(sp^3)	0.0	0.5	0.5
M—N(sp^2)—C(sp^2)=O	0.0	1.5	0.0

[a] The force constants used for the ligand part of the complexes were "final value quality" from the Amber program contained in the MacroModel package, Version 3.0 (see Experimental Section). However, the torsional parameters for the N(sp^2)—C(sp^3)—C(sp^2)—OH and N(sp^2)—C(sp^3)—C(sp^2)=O angles for the $[TcO(MAG_3H)]^-$ and $[TcO(MAG_3)]^{2-}$ complexes were as follows: V1 = V3 = 0, V2 = 0.5 kcal/mol (to fit the X-ray structure); or V1 = V3 = 0, V2 = 0.067 kcal/mol (in agreement with the MacroModel force fields, see text). [b] $E_b = \sum(\text{bonds})K(R - R_0)^2$. [c] $E_\theta = \sum(\text{angles})K(\theta - \theta_0)^2$. [d] Atom type from MacroModel.[28]

Results

The isomeric N_3S ligands were synthesized by standard methods of peptide chemistry (Figure 1). The aminobenzoic acid moieties (I) were first coupled with glycine via an acyl chloride. An acyl chloride (II) was chosen because the aminobenzoic acids are less nucleophilic than common α-amino acids and the usual activated ester coupling procedure gave poor results. The deprotected "dipeptides" (IV) were then coupled to V to afford the *S*-benzoyl (SBz) esters (VI), which readily hydrolyzed to the desired ligands during complexation.

trans-$[Re(V)O_2(en)_2]^+$ has been used as a Re(V) precursor in the synthesis of $Re^VO\text{–}N_2S_2$ and $Re^VO\text{–}N_3S$ complexes at high pH and temperature (pH ≥ 10, 90 °C).[2,4] The complex $Re^VOCl_3(Me_2SO)(Ph_3P)$[16] is easily prepared and isolated and has been shown to react with neutral nitrogen donor ligands (en, py) to give *trans*-$[Re^VO_2N_4]^+$ species. These results demonstrate that the nonchelating ligands of $Re^VOCl_3(Me_2SO)(Ph_3P)$ act as rel-

(28) Still, W. C. et al. MacroModel V3.0. Department of Chemistry, Columbia University, New York.
(29) Jones, A. G.; DePamphilis, B. V.; Davison, A. *Inorg. Chem.* **1981**, *20*, 1617.
(30) Cini, R.; Giorgi, G.; Laschi, F.; Rossi, C.; Marzilli, L. G. *J. Biomol. Struct. Dyn.* **1990**, *7*, 859.

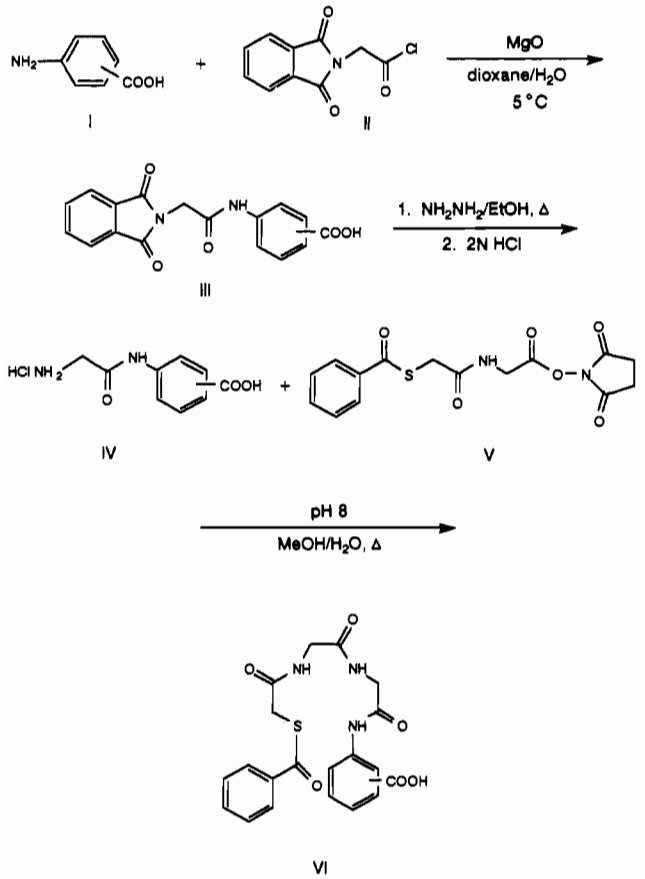

Figure 1. Synthesis of isomeric $SBzMAG_2$-$ABAH_5$ protected ligands.

atively good leaving groups. Therefore, $ReOCl_3(Me_2SO)(Ph_3P)$ instead of *trans*-$[ReO_2(en)_2]^+$ was investigated to prepare Re^V-O-N_3S complexes. $ReOCl_3(Me_2SO)(Ph_3P)$ reacted smoothly with the $SBzMAG_2$-$ABAH_5$-protected ligands under moderate conditions (pH 8, 65–70 °C), producing the orange $[ReO(MAG_2$-$ABAH)]^-$ anions of **8–10**, which were isolated as $[Ph_4P]^+$ or $[Bu_4N]^+$ salts.

All three Re(V) (d^2) complexes absorb weakly in the visible region at 400 and 483 nm. However, the low solubility of the ortho complex in organic solvents precluded determination of extinction coefficients. The FTIR spectra show strong bands at 966, 977, and 970 cm^{-1} for the ortho, meta, and para complexes, respectively. Intensities and frequencies of the bands are characteristic of $Re^V{=}O$ stretching frequencies in Re(V) monooxo complexes.[31] The ^1H NMR spectra, ^{13}C NMR spectra, and elemental analyses are consistent with the assigned chemical formulas and structures.

The ^1H NMR spectra display doublets of doublets for CH_2 groups. Coupling between geminal protons (17–18 Hz) is observed because the oxo ligand creates an unsymmetrical environment. The chemical shifts of corresponding methylene protons in the para and meta complexes are nearly identical (±0.02 ppm) while those of the ortho complex are slightly upfield (≤0.13 ppm).

The ^{13}C NMR spectra of the complexes are also remarkably similar; signals of the corresponding chelate ring carbons (CO and CH_2) usually vary by 0.25 ppm or less. However, one CO signal of the ortho complex is downfield 0.8 and 1.0 ppm from the signals of the meta and para complexes, respectively. These signals are assigned to the CO closest to the benzoate terminus. Such an assignment is consistent with deshielding by the carboxyl group, with the effect diminishing with increasing distance between the groups.

In general, the coordination shift $\Delta = \delta_i(\text{complex}) - \delta_i(\text{free})$ (where δ_i = shift of any corresponding C) is positive (downfield). The chelate ring carbon signals have the largest Δ's; >20 ppm for the amide carbonyl signals and 5–13 ppm for the methylene carbon signals. In studies of tripeptide complexes with Pt(II)[32] and Co(III),[33] Δ values for the ^{13}C signals of the carbonyl and methylene carbons were also positive. However, the magnitude of Δ for the carbonyl signals was modest for the Pt(II) and Co(III) complexes: <10 ppm except for the CO_2^- groups.

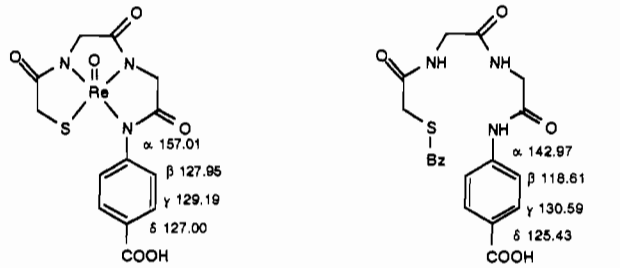

Figure 2. ^{13}C NMR chemical shift assignments (ppm) for the aromatic carbon atoms of $[ReO(MAG_2$-$pABAH)]^-$ (anion of **8**) and the protected ligand, $SBzMAG_2$-$pABAH_5$ (**4**).

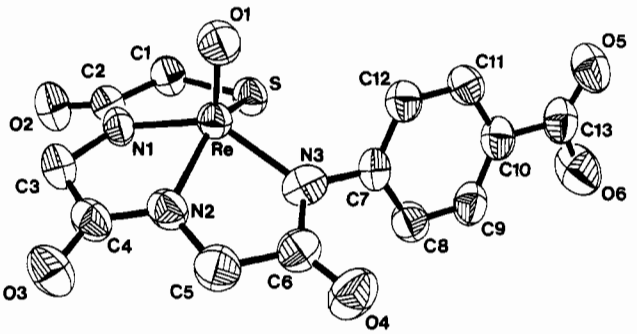

Figure 3. Perspective drawing of $[ReO(MAG_2$-$pABAH)]^-$ (anion of **8**) with 50% probability for the thermal ellipsoids.

The aromatic carbon signals of the free ligands were assigned by predicting δ_i with the equation: $\delta_i(C_6H_{6-n}X_n) = 128.5(\delta(C_6H_6) + \sum Z_i$ ppm.[34] The substituent increments Z_i for COOH and $NHCOCH_3$ were obtained from monosubstituted benzenes and thus do not take into account any interaction between substituents in multisubstituted benzenes. However, assignment of the well-separated signals was straightforward.

Aromatic carbon signal assignments by inspection were possible only for the para complex (**8**) because the aromatic group has time-averaged two-fold symmetry and only four signals (Figure 2). The two weaker signals were assigned to quaternary carbons with specific assignments based on the large difference in shifts. The more downfield remaining signal was assigned to the γ carbons ortho to the electron-withdrawing carboxyl group. It is evident that the signals of the aromatic carbons ortho and para to the amide group in **8** have shifted downfield: Δ_{ortho} = 9.34 ppm and Δ_{para} = 1.57 ppm (Figure 2). For the meta (**9**) and ortho (**10**) complexes, the signals for the unsubstituted carbons are closely clustered around 128.5 ppm. Although specific assignments have not been made, a general downfield shift in the signals is observed. This trend indicates that the electron-donating ability of the amide group is reduced when the H atom is replaced by the Re atom; hence, the signals of the carbon atoms in positions ortho and para to the amide group shift downfield. The signals of the amide-substituted carbons also shift downfield; Δ = 13–14 ppm for all three isomers. The aromatic resonances in $[Co(NH_3)_2$(gly-gly-*l*-phe)][33] are also deshielded (Δ 0.17–0.88 ppm); this has been attributed at least in part to increased electron delocalization in the peptide backbone on chelation.

The structures of $[Ph_4P][ReO(MAG_2$-$pABAH)]\cdot H_2O$ (**8**) and $[Ph_4P][ReO(MAG_2$-$oABAH)]$ (**10**) were determined by X-ray diffraction. Perspective drawings of the anions of **8** and **10** are

(31) Nugent, W. A.; Mayer, J. M. *Metal Ligand Multiple Bonds*; Wiley: New York, 1988; p 116.

(32) Kirvan, G. E.; Margerum, D. W. *Inorg. Chem.* **1985**, *24*, 3017.

(33) Evans, E. J.; Grice, J. E.; Hawkins, C. J.; Heard, M. R. *Inorg. Chem.* **1980**, *19*, 3496.

(34) Breitmaier, E.; Voelter, W. *Carbon-13 NMR Spectroscopy*; VCH Publishers: New York, 1987; p 254.

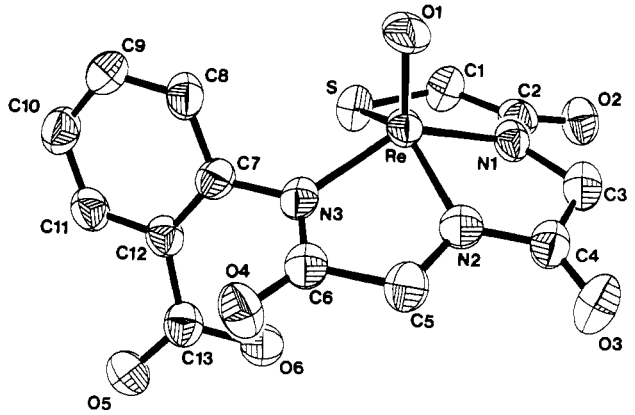

Figure 4. Perspective drawing of $[ReO(MAG_2\text{-}oABAH)]^-$ (anion of **10**) with 50% probability for the thermal ellipsoids.

Table V. Selected Geometrical Parameters for $[ReO(MAG_2\text{-}pABAH)]^-$ (Anion of **8**) and $[ReO(MAG_2\text{-}oABAH)]^-$ (Anion of **10**)

	$[ReO(MAG_2\text{-}pABAH)]^-$		$[ReO(MAG_2\text{-}oABAH)]^-$	
	X-ray	calcd	X-ray	calcd
	Bond Distances (Å)			
Re-O(1)	1.670 (5)	1.659	1.684 (4)	1.657
Re-S	2.283 (2)	2.291	2.295 (2)	2.290
Re-N(1)	1.987 (5)	2.011	2.012 (5)	2.010
Re-N(2)	1.984 (5)	1.996	1.976 (4)	1.996
Re-N(3)	2.024 (6)	2.052	2.019 (6)	2.050
	Bond Angles (deg)			
S-Re-O(1)	110.5 (2)	109.6	110.9 (1)	109.6
S-Re-N(1)	82.4 (2)	83.3	82.6 (1)	83.4
S-Re-N(2)	135.6 (2)	136.4	136.2 (1)	136.4
S-Re-N(3)	92.1 (2)	91.9	92.4 (1)	91.7
O(1)-Re-N(1)	110.2 (2)	109.5	110.0 (2)	109.7
O(1)-Re-N(2)	113.6 (3)	113.7	112.6 (2)	113.7
O(1)-Re-N(3)	109.7 (2)	109.4	109.0 (2)	109.7
N(1)-Re-N(2)	78.0 (2)	78.0	78.5 (2)	78.1
N(1)-Re-N(3)	139.0 (2)	140.0	139.9 (2)	139.7
N(2)-Re-N(3)	78.1 (2)	78.6	78.0 (2)	78.3
Re-S-C(1)	100.1 (2)	98.9	99.5 (2)	98.9
Re-N(1)-C(2)	125.7 (4)	121.4	124.9 (4)	121.3
Re-N(1)-C(3)	115.9 (4)	116.7	115.5 (4)	116.7
Re-N(2)-C(4)	119.3 (5)	117.9	120.1 (4)	117.9
Re-N(2)-C(5)	119.5 (5)	118.5	119.4 (4)	118.4
Re-N(3)-C(6)	118.3 (5)	115.4	118.3 (5)	115.6
Re-N(3)-C(7)	123.9 (4)	123.7	123.5 (4)	123.5

presented in Figures 3 and 4. Selected bond lengths and angles are presented in Table V. Both complexes are square pyramidal. The rhenium atom is displaced 0.74 (**8**) and 0.73 Å (**10**) above the basal plane defined by the ligand donor atoms: S, N(1), N(2), N(3). (The mean deviation from the basal plane is 0.055 Å in both structures.) The dihedral angle between the basal plane and the plane defined by the phenyl ring is 70.9° in **8** and 105.3° in **10**. The Re-O bond distances for **8** (1.670 (5) Å) and **10** (1.684 (4) Å), the Re-S bond distances for **8** (2.283 (2) Å) and **10** (2.295 (2) Å) and the ranges of Re-N bond distances for **8** (1.984-2.024 Å) and **10** (1.976-2.019 Å) are normal[4,13,35] and do not deviate appreciably from the bond distances reported for the N_3S complex $[ReO(MAG_3H)]^-$: Re-O, 1.68 (1) Å; Re-S, 2.285 (7) Å; Re-N, 1.98-2.04 Å.[2] The orientation of the carboxyl group in **10** is anti to the Re=O group. An anti orientation is also found in the structure of $[ReO(MAG_3H)]^-$.

The carboxyl hydrogen atoms were located in each structure and one water molecule per asymmetric unit was located for **8**. There is evidence of intermolecular hydrogen bonding involving these atoms in both structures. Contacts for **8** include the following: O(2)-H_aO(7)H_b, 1.837 Å; H_aO(7)H_b-O(4) (symmetry position $-x, -y + 1, -z$), 1.981 Å; O(7)-H(carboxyl) (symmetry position $x - 1, y, z - 1$), 1.985 Å. The contact for **10** is H(carboxyl)-O(2) (symmetry position $x, -y + {}^1/_2, z - {}^1/_2$), 1.804 Å. There is no evidence of bonding to the metal-oxo groups by the carboxyl groups or the water molecule.

Table VI. Total Strain Energies for the Computed Minimum Energy Structures of the Re/Tc Complexes

complex	E_{tot}, kcal/mol	
$[ReO(MAG_2\text{-}pABAH)]^-$	19.41[a]	
$[ReO(MAG_2\text{-}oABAH)]^-$	20.31[a]	
$[ReO(MAG_2\text{-}pABA)]^{2-}$	19.46[a]	
anti-$[ReO(MAG_2\text{-}oABA)]^{2-}$	19.98[a]	
syn-$[ReO(MAG_2\text{-}oABA)]^{2-}$	20.65	
syn-$[ReO(MAG_2\text{-}mABA)]^{2-}$	19.31	
anti-$[ReO(MAG_2\text{-}mABA)]^{2-}$	19.12	
syn-$[TcO(MAG_3H)]^-$	10.00[c]	11.62[a,b]
anti-$[TcO(MAG_3H)]^-$	10.12[c]	10.92[b]
syn-$[TcO(MAG_3)]^{2-}$	9.77	10.79[a,b]
anti-$[TcO(MAG_3)]^{2-}$	9.85	10.19[b]
anti-$[ReO(MAG_3H)]^-$	10.16[a]	

[a] Conformation similar to that of an X-ray structure. [b] Values derived from the V1 = V3 = 0, V2 = 0.5 kcal/mol set of torsional constants for the N(sp2)-C(sp3)-C(sp2)-OH and N(sp2)-C(sp3)-C(sp2)=O angles to fit the X-ray structure (see text). [c] The syn conformer has the OH distal from Tc. The proximal conformer has E_{tot} = 10.37 kcal/mol. The same final geometry is distal for the anti species regardless of initial OH location (proximal or distal).

The gas phase structures of both monoprotonated complexes ($[ReO(MAG_2\text{-}pABAH)]^-$, $[ReO(MAG_2\text{-}oABAH)]^-$, $[ReO(MAG_3H)]^-$, and $[TcO(MAG_3H)]^-$) and fully deprotonated complexes ($[ReO(MAG_2\text{-}pABA)]^{2-}$, $[ReO(MAG_2\text{-}oABA)]^{2-}$, $[ReO(MAG_2\text{-}mABA)]^{2-}$, and $[TcO(MAG_3)]^{2-}$) were computed using molecular mechanics calculations (Table VI). Minimum energy structures were calculated for both syn and anti orientations of the deprotonated complexes (when applicable) and for $[TcO(MAG_3H)]^-$.

The Tc(V)/Re(V) centers have a d^2 configuration (B_2^2 microstate for the C_{4v} point group of an ideal square pyramidal coordination sphere). The directional properties of this configuration were, to some extent, accounted for by including in the calculations bending and torsional terms for those angles that directly involve the metal ion.[23,25,26,36] It was previously found that the inclusion of bending and torsional terms associated with the metal-donor bonds can partially simulate the 1,3-interactions in the coordination sphere.[26]

All the calculated and found bond distances and angles agree within 0.04 Å (and usually within less than 0.025 Å) and 6°, respectively, for $[ReO(MAG_2\text{-}pABAH)]^-$ (RMS = 0.010 Å), $[ReO(MAG_2\text{-}oABAH)]^-$ (RMS = 0.019 Å) (Table V). The calculated *syn*-$[TcO(MAG_3H)]^-$ structure also has a good superimposition with the X-ray structure (RMS = 0.009 Å). (However, see discussion below.) From the good agreement of the geometrical parameters (Table V), it is evident that the force fields adopted in the present investigation allow us to compute faithfully the structures of this class of Re(V) and Tc(V) species. The total strain energies for all the Re(V) and Tc(V) structures are reported in Table VI.

anti-$[ReO(MAG_2\text{-}oABAH)]^-$ is destabilized about 0.90 kcal/mol with respect to the para analogue owing to the repulsive interaction of the ortho COOH group with the coordination sphere atoms. Similarly, the $[ReO(MAG_2\text{-}pABA)]^{2-}$ dianion is 0.5 kcal/mol more stable than the $[ReO(MAG_2\text{-}oABA)]^{2-}$ dianion. The ortho COO^- group is located anti to the apical oxygen donor with respect to the C(7)-N(3)-Re plane. The strain energy of *syn*-$[ReO(MAG_2\text{-}oABA)]^{2-}$ is some 0.70 kcal/mol higher than that of the anti form. Large repulsive nonbonding interactions between the COO^- group and the coordination sphere atoms are responsible for the destabilization. The barrier between the syn and anti minima is greater than 20 kcal/mol.

(35) Mattes, R.; Weber, H. *Z. Anorg. Allg. Chem.* **1981**, *474*, 216.

(36) Drew, M. G. B.; Hollis, S.; Yates, P. C. *J. Chem. Soc., Dalton Trans.* **1985**, 1829.

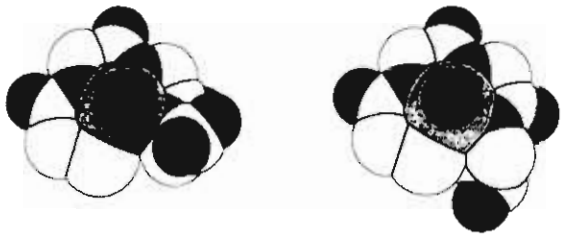

Figure 5. Space filling models of *syn*-$[TcO(MAG_3)]^{2-}$ (left) and *anti*-$[TcO(MAG_3)]^{2-}$ (right) calculated with normal torsional parameters (V1 = V3 = 0, V2 = 0.067 kcal/mol).[28]

anti-$[ReO(MAG_2\text{-}mABA)]^{2-}$ has an energy value only 0.15 kcal/mol lower than that of $[ReO(MAG_2\text{-}pABA)]^{2-}$, while *syn*-$[ReO(MAG_2\text{-}mABA)]^{2-}$ is 0.34 kcal/mol more stable than $[ReO(MAG_2\text{-}pABA)]^{2-}$. The small stabilization of the meta derivatives with respect to the para one is due to weak attractive van der Waals contributions between the COO^- group and coordination sphere atoms.

The $COOH/COO^-$ groups are almost coplanar with the aromatic ring for all the para and meta complex molecules, for both the observed and calculated structures. However, in the structures of the ortho derivatives the dihedral angles involving the carboxyl group and phenyl ring exhibit large deviations from coplanarity (20–40°). This deviation is due to the steric hindrance between the carboxyl group and coordination sphere.

The minimized structure of *syn*-$[TcO(MAG_3H)]^-$ that agrees with the twisted X-ray structure was obtained by using the high value for a torsional potential (V1 = V3 = 0; V2 = 0.5 kcal/mol) for the $N(sp^2)—C(sp^3)—C(sp^2)—OH$ and $N(sp^2)—C(sp^3)—C(sp^2)=O$ torsion angles. This value is an order of magnitude greater than the values usually adopted for these types of torsion angles.[28] However, the existence of an intermolecular hydrogen bond involving the COOH group and the carbonyl O(2) oxygen atom can explain why a large constant for the torsional potential was needed to obtain a geometry which superimposed well on the distorted X-ray structure. The calculated strain energy of the *syn*-$[TcO(MAG_3H)]^-$ gas-phase species with the X-ray geometry is 0.7 kcal/mol higher than that calculated for *anti*-$[TcO(MAG_3H)]^-$. The barrier between the anti and syn minima is higher than 12 kcal/mol. Similarly, calculated strain energies of the deprotonated forms in the gas phase show that the anti conformation is again more stable (0.6 kcal/mol) than the syn conformation.

The syn and anti forms of $[TcO(MAG_3)]^{2-}$ (Figure 5) and $[TcO(MAG_3H)]^-$ were recalculated using reasonable values for the potentials of $N(sp^2)—C(sp^3)—C(sp^2)—OH$ and $N(sp^2)—C(sp^3)—C(sp^2)=O$ torsion rotations in the original Amber force field (V1 = V3 = 0; V2 = 0.067 kcal/mol).[28] The minimized structure of *syn*-$[TcO(MAG_3H)]^-$ is reasonable with regard to the orientation of the carboxyl group. The $N–CH_2–C(O)–OH$ dihedral angle is 21° for the X-ray structure, while the angle is −66° in the absolute minimum of the newly calculated structure. Calculations suggest that rotating the COOH group around the $CH_2–COOH$ bond to obtain the twisted geometry of the solid-state structure requires about 6 kcal/mol. This result suggests that strong hydrogen bonds in the $[Ph_4As][TcO(MAG_3H)]$ crystal lattice[5] are responsible for the displacement of the COOH from its most favorable position.

The total strain energies for the structures minimized with both force fields are reported in Table VI. Both the protonated and deprotonated forms have syn and anti conformations with similar energy values.

Discussion

The present study provides two well-defined $Re^VO–N_3S$ crystal structures: $[Ph_4P][ReO(MAG_2\text{-}pABAH]\cdot H_2O$ (**8**) and $[Ph_4P][ReO(MAG_2\text{-}oABAH]$ (**10**). The structures confirmed the expected Re coordination sphere: square pyramidal with an apical oxo ligand. Corresponding bond lengths and angles associated with the chelate portion of the molecule do not differ more than 0.03 Å and 2°, respectively, between the two complexes. Electronic, ^1H NMR, and ^{13}C NMR spectra also indicate similar coordination environments. Thus, the only significant structural variable is the position of the carboxyl group, which is probably responsible for any difference in the biological distribution of the analogous ^{99m}Tc complexes.

We have been able to explore the effects of the carboxyl position on the structures and energies of these complexes using molecular mechanics investigations. The first goal of the molecular mechanics investigation was to generate structures of the complexes with an ionized carboxyl group because the deprotonated species more closely approximates structures of the complexes present in vivo. We first developed a force field to fit the solid-state geometries, although caution must be exercised to account for solid-state effects. Reasonable values for the parameters must be used.

The importance of predicting structures has been borne out in the investigation of the $MO(MAG_3)$ complexes. A twisted syn conformation is adopted in the solid-state structure of $[TcO(MAG_3H)]^-$.[5] Fitting the unfavorable torsion angle ($N–CH_2–C(O)–OH$) requires unusually large values for torsional parameters. Even with such an adjustment, an anti conformation is more favorable. Indeed, an anti conformation is adopted in the crystal structure of $[ReO(MAG_3H)]^-$,[2] and the observed solid-state structure is close to the minimum energy geometry for the gas phase (RMS = 0.019 Å), as calculated on the basis of normal torsional potentials. Further analysis indicates that syn and anti conformations of $[TcO(MAG_3)]^{2-}$ (Figure 5) or $[TcO(MAG_3H)]^-$ calculated with normal torsional terms have very similar absolute energies; this finding suggests that there is not an energetically preferred conformation for either isolated anion. The twisted syn geometry of $[TcO(MAG_3H)]^-$ found in the crystal lattice is different from the syn geometry predicted; this twisting is a consequence of an intermolecular hydrogen bond involving the protonated carboxyl group. Therefore, the solid-state structure of $[TcO(MAG_3H)]^-$ appears to be a poor model for the expected solution-phase structure of $[TcO(MAG_3)]^{2-}$.

The second goal of the molecular mechanics investigation was to determine whether the distance between the oxo ligand and the carboxyl group in the deprotonated species had any correlation with the renal clearance of the ^{99m}Tc analogues. Of course, the oxo–carboxyl distance will vary with conformation in the ortho and meta derivatives. Furthermore, in the related complexes $[TcO(mapH)]^-$ and $[ReO(mapH)]^-$, two epimers with the carboxyl group either syn or anti to the oxo group are known.[4] The syn epimer of $[^{99m}TcO(map)]^{2-}$ is cleared by the kidneys faster than the anti epimer, and it has been postulated that the anion transport mechanism recognizes the complex more easily when the carboxyl group is on the same side as the oxo group.[37] Therefore, it was important to determine if an energetically preferred conformation for the ortho and meta complexes exists and to consider the oxo–carboxyl distance when formulating structure–distribution relationships.

The oxo–carboxyl distances for the deprotonated species $[MO(MAG_2\text{-}ABA)]^{2-}$, along with the corresponding distances in $[MO(MAG_3)]^{2-}$ in its minimum energy geometry, were calculated for comparison. The distances $O_{oxo}–C$, $O_{oxo}–O_{proximal}$ and $O_{oxo}–O_{distal}$ for each complex are collected in Table VII. The oxo–carboxyl distances in the solid-state structures of monoprotonated *syn*-$[TcO(mapH)]^-$ and *anti*-$[TcO(mapH)]^-$[4] are also listed in Table VII. The distances estimated for *syn*-$[MO(MAG_3)]^{2-}$ are about 1.5 Å shorter than for the anti conformer. These distances can be compared to some of the less conformationally flexible species in Table VII.

We have not estimated the solution-phase structures through calculations on $[MO(map)]^{2-}$ in the gas phase, but for these relatively rigid epimers, the structure should not be very phase dependent. We approximate these distances as being those of the $[TcO(mapH)]^-$ epimers. The oxo–carboxyl distances of the

(37) Klingensmith, W. C.; Fritzberg, A. R.; Spitzer, V. M.; Johnson, D. L.; Kuni, C. C.; Williamson, M. R.; Washer, G.; Weil, R. *J. Nucl. Med.* **1984**, *25*, 42.

Table VII. Oxo–Carboxyl Interatomic Distances (Å) Calculated or Estimated for Geometries of Fully Ionized Tc/Re Complexes

complex	O_{oxo}–C	O_{oxo}–$O_{proximal}$	O_{oxo}–O_{distal}
$MO(MAG_2\text{-}pABA)]^{2-}$	7.5	7.8	8.5
syn-$[MO(MAG_2\text{-}mABA)]^{2-}$	5.6	5.0	6.8
anti-$[MO(MAG_2\text{-}mABA)]^{2-}$	7.6	7.9	8.5
syn-$[MO(MAG_2\text{-}oABA)]^{2-}$	3.6	3.4	4.1
anti-$[MO(MAG_2\text{-}oABA)]^{2-}$	5.8	5.3	7.0
syn-$[MO(MAG_3)]^{2-}$ [a]	3.6	3.5	4.2
anti-$[MO(MAG_3)]^{2-}$ [a]	5.3	4.9	5.6
syn-$[MO(map)]^{2-}$ [b]	4.7	4.2	5.9
anti-$[MO(map)]^{2-}$ [b]	5.2	5.4	6.2

[a] Minimum energy geometry (see text). [b] Estimated as being the same as those found in the X-ray structures of the $[TcO(mapH)]^-$ anions.[4]

$[MO(map)]^{2-}$ epimers are slightly longer than the corresponding distances in *syn*-$[MO(MAG_3)]^{2-}$. The differences, which are ≤2 Å but significant, may explain why both $[TcO(map)]^{2-}$ epimers are secreted less efficiently than $[TcO(MAG_3)]^{2-}$ by the anion transport system[38] and why the syn epimer is secreted more efficiently than the anti epimer. Both epimers have distances more similar to *anti*-$[MO(MAG_3)]^{2-}$, suggesting that it is *syn*-$[MO(MAG_3)]^{2-}$ that is secreted.

The oxo–carboxyl distances in *syn*-$[MO(MAG_2\text{-}oABA)]^{2-}$ are nearly identical to the oxo–carboxyl distances in *syn*-$[MO(MAG_3)]^{2-}$. However, in both the syn and anti forms, the ortho isomer is destabilized due to the repulsive interaction of the carboxyl group and the metal coordination sphere. The strain energy is somewhat moderated by an anti relationship between the carboxyl group and M=O core. The calculated rotational barrier (>20 kcal/mol) about the N(3)–C(7) bond and the single species present in the ^1H NMR spectra suggest that the anti conformation is maintained in solution at room temperature. This preference of the anti conformation may explain the poor renal clearance of the ortho complex despite potentially ideal oxo–carboxyl distances of the syn conformer. The ortho isomer has distances similar to *anti*-$[MO(MAG_3)]^{2-}$ and its poor biodistribution suggests again that the syn conformer of $[MO(MAG_3)]^{2-}$ is secreted.

The oxo–carboxyl distances in the anti conformer are very close to those of the para isomer (Table VII). However, the calculations suggest that the meta isomer is in the syn conformation about half the time in the gas phase. If the energy relationships hold in solution, the time-averaged difference in the oxo–carboxyl distances (Table VII) may contribute to the threefold difference in the renal clearance of the meta and para complexes of ^{99m}Tc.[12]

The oxo–carboxyl distances in the para complex (Table VII) are approximately 4 and 2–3 Å longer, respectively, than in the syn and anti conformers of the clinically used prototype, $[^{99m}TcO(MAG_3)]^{2-}$. This suggests that there may be at least two separate binding modes for anion transport. Multiple renal secretory systems for organic anions have been suggested.[39] The longer distances in the para isomer may simply correspond to electron-deficient regions in the binding site of this other transport receptor. Therefore, construction of $[^{99m}TcO(MAG_3)]^{2-}$ analogues with the longer oxo–carboxyl distance may produce useful renal agents. Alternatively, the oxo–carboxyl distance may not be the key structural parameter for efficient renal transport.

Conclusions

The structural characterization of Re complexes with mercaptoacetylglycylglycylaminobenzoic acid ligands has provided well-defined information about the $Re\text{–}N_3S$ system. In addition, this isomeric ligand series has allowed us to assess the effects of the carboxyl position on the renal clearance of their ^{99m}Tc metal chelates through structural characterization and molecular mechanics calculations on the Re complexes. Specifically, we were concerned that the MAG_3 complexes were too conformationally flexible to define the position of the carboxyl group. Both our calculations and considerations of the reported structures of the Tc and Re complexes support this concern. The comparison of contributions to biodistributions of the analogues suggests that *syn*-$[^{99m}TcO(MAG_3)]^{2-}$ is transported. However, a second renal secretory system may explain the transport of $[^{99m}TcO(MAG_2\text{-}pABA)]^{2-}$. Since clearly defined structures are critical to the design of improved ^{99m}Tc and $^{186}Re/^{188}Re$ radiopharmaceuticals, further assessment of $^{99m}TcO(MAG_2\text{-}ABA)$ complexes appears warranted. For example it would be worthwhile to construct an ortho derivative with a syn conformation. Although the use of gas-phase calculations with solution-phase and solid-phase correlations must be considered to be preliminary, the overall approach appears promising for radiopharmaceutical design.

Acknowledgment. We thank Rene Lachicotte and Karl S. Hagen for help with the crystallographic studies and we gratefully acknowledge financial support from the National Institutes of Health (Grant No. DK38842-04).

Supplementary Material Available: Figures showing ^{13}C NMR chemical shift assignments for the aromatic carbons of **4**–**6**, stereoviews of **8** and **10**, and space-filling models of observed and calculated **8** and **10** and tables of analytical and ^1H NMR data for compounds **1**–**6**, crystallographic data for **8** and **10**, observed and calculated (anion only) geometrical parameters for **8** and **10**, H-atom coordinates and isotropic displacement coefficients for **8** and **10**, anisotropic displacement coefficients for **8** and **10**, and least-squares planes of **8** and **10** (18 pages); tables of observed and calculated structure factors for **8** and **10** (32 pages). Ordering information is given on any current masthead page.

(38) Taylor, A.; Eshima, D.; Fritzberg, A. R.; Kasina, S.; Christan, P. E. *Contrib. Nephrol.* **1986**, *56*, 5.

(39) Hewitt, W. R.; Wagner, P. A.; Bostwick, E. F.; Hook, J. B. *J. Pharmacol. Exp. Ther.* **1977**, *202*, 711.